Stretch-Modulated Carbon Nanotube Alignment in Ferroelectric Polymer Composites: Characterization of the Orientation State and Its Influence on the Dielectric Properties

ARTICLE *in* THE JOURNAL OF PHYSICAL CHEMISTRY C · SEPTEMBER 2011

Impact Factor: 4.77 · DOI: 10.1021/jp205444x

THE JOURNAL OF PHYSICAL CHEMISTRY C

ARTICLE

pubs.acs.org/JPCC

Stretch-Modulated Carbon Nanotube Alignment in Ferroelectric Polymer Composites: Characterization of the Orientation State and Its Influence on the Dielectric Properties

Sheng-Hong Yao,[‡,§] Jin-Kai Yuan,[‡] Tao Zhou,[§] Zhi-Min Dang,[*,†,§] and Jinbo Bai[*,‡]

[†]Department of Polymer Science and Engineering, University of Science and Technology Beijing, Beijing 100083, People's Republic of China

[‡]Laboratoire de Mécanique des Sols, Structures et Matériaux, Ecole Centrale Paris, CNRS UMR8579, PRES UniverSud, Grande Voie des Vignes, 92290 Châtenay-Malabry, France

[§]State Key Laboratory of Chemical Resource Engineering, Beijing University of Chemical Technology, Beijing 100029, People's Republic of China

ABSTRACT: The large electrically stimulated actuation in high-performance actuator materials requires a careful investigation of how the variation in strain would affect the mechanism of inside polarization and thus the final dielectric properties of the carbon nanotube electroactive composites. Herein, we systematically studied the tensile strain's effect on the dielectric properties of multiwall carbon nanotube (MWNT)/poly(vinylidene fluoride) (PVDF) nanocomposites, by quantitatively characterizing the inside microstructure shift during uniaxial mechanical stretching. The results showed that MWNTs became aligned in response to the external stretching and the preferential alignment degree increased with the tensile strain. This in turn triggered a complex changing law of macroscopic dielectric properties. Maximum increment in the dielectric permittivity of the composite can reach 30% at 10^2 Hz relative to that before stretching. Evolution of conductive pathways and formation of microcapacitors during stretching can be invoked as being responsible for the large variation of dielectric properties. This was finally confirmed by using an equivalent circuit model of two parallel *RC* circuits in series to analyze the impedance data.

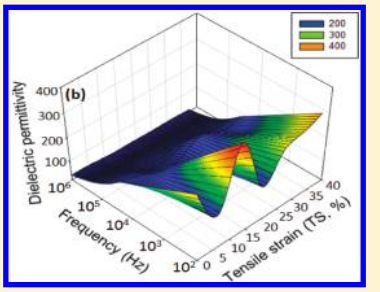

INTRODUCTION

Carbon nanotubes (CNTs) are currently of intense interest as highly promising building block for manufacturing nanostuctured low-cost and high-performance polymer composites. This increasing interest stems from their nanometer-scale dimension, along with their large shape anisotropy and a unique combination of exotic mechanical, thermal, and electrical properties.[1−5] As compared to the polymer matrices, CNT composites show significant improvement in tensile modulus,[6] thermal conductivity,[7] electrical conductivity,[8,9] and dielectric properties.[10−12] Very recently, CNT composites with high dielectric permittivity (ε_r) have been invested with tremendous research efforts to improve the electromechanical response of high-performance actuators and sensors.[13,14] In this field, electroactive polymers, such as poly(vinylidene fluoride) (PVDF) and poly(vinylidene fluoride-trifluoroethylene) [P(VDF-TrFE)] copolymer, are often chosen as host polymers because of their ability to perform efficient electrical-to-mechanical energy conversion and respond to external electrical stimulation by generating large mechanical actuations.[13−16] To improve the electromechanical strain and energy density of such polymers further, the key issue is to raise the overall dielectric permittivity meanwhile retaining the intrinsic flexibility of polymers. Preliminary studies have demonstrated that introducing CNTs into polymers to form a random-network structure could be a promising strategy to meet this end. An ultrahigh dielectric permittivity can be predicted by the implementation of percolation theory just below the threshold,[11−14,17] accordingly enhancing the strain response at a reduced driving electric field.[13,14] Additionally, the high thermal conductivity of CNTs can improve the heat dissipation and quickly release the undesired heat generated by loss tangent, thus preventing materials from dielectric breakdown.[13,18] More importantly, these improvements are achieved at a very low loading due to the extremely high aspect ratio of CNT.

Despite tremendous progress toward understanding the CNT's effect on dielectric behaviors of polymer composites, most of the reported studies either challenged the uniform dispersion of CNTs in polymer matrices, or revealed the mechanisms of the high dielectric permittivity and/or large electromechanical actuations. However, little was found on the dependence of the dielectric properties on the extensive external fields such as force (tensile strain) and electric and magnetic field. It has been demonstrated that these external fields played a crucial role in defining the internal microstructure of composites, such as molecular arrangement of polymers and the spatial distribution of CNT fillers, which in turn highly affected the macroscopic physical properties of composites.[19−24] For

Received: June 10, 2011
Revised: August 15, 2011
Published: September 07, 2011

example, Chio et al.[20] prepared an aligned CNT/epoxy composite by using a 25 T magnetic field processing. The thermal and electrical conductivities along magnetic field alignment direction were increased by 10% and 35%, respectively, relative to those of randomly oriented CNT composites. Although several studies reported that a unidirectional stretching would also induce the alignment of CNTs in polymer matrices,[19,24] establishing a correlation of the degree of tube alignment with dielectric properties still remains challenging due to the lack of an effective characterization of the CNT orientation states at different tensile strains.

In this work, we prepared a CNT/PVDF nanocomposite loaded with multiwall CNT (MWNT) at 2 wt % (slightly higher than the percolation threshold, f_c = 1.8 wt %)[24,25] and aligned the CNTs inside the polymer matrix by uniaxial mechanical stretching. The alignment degree of tube was varied by controlling the tensile strain (TS) applied on the composite. The orientation states of MWNTs at different TSs were fully quantified by employing an orientation tensor description and further graphically presented with elongated ellipses. The alignment degree of the tube was well correlated with the evolution of dielectric properties of composites. This research may provide a helpful guidance for the development of eletroactive composites into practical applications, where a large actuation (strain) would be stimulated and might greatly affect the dielectric properties.

EXPERIMENTAL SECTION

The MWNTs were synthesized by a chemical vapor deposition (CVD) method, provided by Shenzhen Nanotech Port Company (China). Their diameter was on the order of 20−40 nm, and the length was in the range 5−15 μm. Semicrystalline polymer PVDF was used as host polymer due to its superior ferroelectric nature. The MWNT/PVDF nanocomposites were prepared via solution casting, followed by hot-pressing technology. The MWNT mass concentration used in this study was 2.0 wt %. Without further purification, MWNTs at an appropriate amount were mixed with a solvent [*N*,*N*-dimethylformamide (DMF)] and pulsated in ultrasonic water bath for 2 h. Meanwhile, PVDF powder was dissolved in the DMF solvent at 50 °C. Then, the MWNT suspension was added into PVDF solution and ultrasonically treated for another 10 min. Afterward, the solution was heated at 60 °C for 8 h to completely remove the solvent. The resultant composite films were then folded and molded by a hot-pressing technique at 200 °C and 15 MPa to prepare 1.0 mm-thick plates. Ultimately, the composite plates were cut into dumbbell-shaped samples with 50.0 mm in length, 1.0 mm in thickness, and 8.5 and 4.0 mm in maximal and minimal widths, respectively.

Tensile tests of the as-prepared dumbbell-shaped samples were conducted on CMT4104 electric tensile tester (SANS, China) according to GB/T 528−1998 (ISO 37, 1994) by employing a tensile rate of 10 mm/min. The MWNT/PVDF nanocomposite was mechanically stretched up to the TS of 6.3%, 12.5%, 18.8%, 25.0%, 31.3%, and 37.5%, respectively, and then the load released. The microstructure of the samples parallel to the tensile-strain direction was examined by transmission electron microscopy (TEM, Hitachi H-800), and the ultrathin sections were sliced by microtome under liquid nitrogen cooling. The dielectric properties of the MWNT/PVDF nanocomposites were measured using an impedance analyzer (Agilent 4294A) in the frequency range from 10^2 to 10^6 Hz at room temperature.

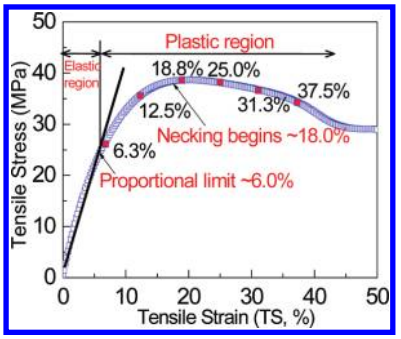

Figure 1. Tensile stress−strain curve of the MWNT/PVDF nanocomposites with f_{MWNT} = 2 wt %.

The impedance magnitude and the impedance phase were measured using an impedance analyzer (Solartron 1260) in a broader frequency range (10^{-3}−10^7 Hz) at room temperature. For a good electrical contact, sample surfaces were painted with silver paste.

RESULTS AND DISCUSSION

Mechanical Behavior of the MWNT/PVDF Nanocomposite. Before investigating the effect of tensile strains on the alignment of MWNTs, it would be of large importance to gain insight into the mechanical behavior of the composites in response to the uniaxial stretching. Figure 1 presents the tensile stress−strain curve of the MWNT/PVDF nanocomposites. (We are not discussing here the improvement of mechanical property imparted from CNT reinforcement in comparison with the neat polymer.) It can be clearly seen that the tensile stress initially increases linearly with the strain until the proportional limit (TS = 6.0%) is reached, which is reconciled with the well-known Hooke's Law. It indicates that in this range (TS < 6.0%) the composite behaves elastically and the deformation can be reversible. On the contrary, from TS = 6.0% on, the stress−strain curve deviates from the straight-line relationship and the law no longer applies as the strain increases faster than the stress. When the stress reaches the ultimate tensile strength, the necking begins in the sample. Hence, in the range TS > 6.0%, the material could not return to its initial undeformed state after unloading and ultimately generates permanent deformation in the composite. Therefore, in this study, the tensile strains uniaxially applied on the samples are controlled to start from 6.3% to 37.5% with an interval of ~6.2%, ensuring all the strains are in the plastic region. That means, after the release of the load, the stretch-induced tubes alignment can be partially retained inside the composites.

Characterization of the Carbon Nanotube Orientation State at Different Tensile Strains. To elucidate a picture of strains' effect on the tube alignment, it is essential to represent the orientation state of MWNTs at different TSs. Development of the orientation tensor description provides an effective way to embody all MWNT directions in the selected region, which has been successfully used to describe the orientation states of short fibers.[26−28] The second moments of the probability distribution function would be adopted in our study, which are called orientation tensors and are defined as the following:[28]

$$\langle a \rangle = \langle p_i p_j \rangle = \oint p_i p_j \varphi(P)\, dP \qquad (1)$$

Here, **P** is the unit vector placed in the average direction of the tube length, as shown in Figure 2a. p_i and p_j are components of

this vector along the coordinate directions. In our study, we apply the orientation tensor description in 2D plane (Figure 2b). Thus in two dimensions

$$p_1 = \sin\theta,\ p_2 = \cos\theta \tag{2}$$

where θ is the orientation angle of a single MWNT. Remarkably, to calculate the components of the orientation tensor $\langle a\rangle$ in the given region, one has to experimentally measure the direction of each MWNT. Being different from the indirect measurement of the CNT directions, such as X-ray,[19] Raman spectroscopy,[29] and polarized light diffraction,[30] the approach used in our study is to digitize MWNT orientation angles directly by microtoming composites as well as detecting all the MWNTs present inside the sections. Vectors are placed in the TEM images and associated with the length direction of each tube, as shown in Figure 3a. The orientation angle of each MWNT is measured by using Image J software. Component a_{ij} in any section where N carbon nanotubes are present is calculated by the equation[28]

$$a_{ij} = \frac{1}{N}\sum_{k=1}^{N} p_i^k p_j^k \tag{3}$$

The orientation tensor results at different TSs are shown in Figure 3. To vividly represent the MWNT alignment, we draw ellipses to graphically describe the orientation state. The parameters of ellipses are automatically obtained by diagonalization from $\langle a\rangle$ to the second order orientation tensor $\langle a\rangle^*$ using the following equation:[28]

$$Q\langle a\rangle Q^T = \begin{bmatrix}\cos\varphi & \sin\varphi\\ -\sin\varphi & \cos\varphi\end{bmatrix}\begin{bmatrix}a_{11} & a_{12}\\ a_{21} & a_{22}\end{bmatrix}\begin{bmatrix}\cos\varphi & \sin\varphi\\ -\sin\varphi & \cos\varphi\end{bmatrix}^T = \begin{bmatrix}a_{11}^* & 0\\ 0 & a_{22}^*\end{bmatrix} = \langle a\rangle^* \tag{4}$$

Here, a^*_{11} and a^*_{22} are the length of major and minor axes of the ellipse, respectively. φ in the rotation matrix $\langle Q\rangle$ is the angle of major axis rotated anticlockwise from horizon axis X. The principle values for $\langle a\rangle^*$ at different TSs are listed in Table 1. The ellipses are drawn accordingly as illustrated in Figure 3. In these ellipses, the values of the major and minor axes describe the degree of orientation in that direction.[26,28] Hence, the major axes represent the direction of preferential alignment of MWNTs, and the preferential alignment degree (PAD) can be quantificationally defined as

$$\mathrm{PAD} = \frac{a_{11}^* - a_{22}^*}{a_{11}^* + a_{22}^*} \tag{5}$$

PADs are also listed in Table 1. The subcircular geometry of the ellipse at TS = 0 (Figure 3a) gives a much lower PAD value (0.08), thus signifying a randomly oriented MWNT structure, namely no particular preference of orientation before stretching. However, after loading (6.3% ≤ TS ≤ 37.5%), the ellipses become more elongated in shape (Figure 3b−e), and the corresponding PADs increase with tensile strain; namely, the MWNT orientation degree can be modulated by controlling the external tensile strains applied on the composite. Of particular interest is that when TS increases from 0 to 6.3% and from 12.5% to 25.0%, the PAD increases drastically from 0.08 to 0.44 and from 0.58 to 0.85, respectively. The MWNT orientation state reacts much sensitively to the composite deformation in these two ranges. Therefore, two conclusions can be drawn: (1) The

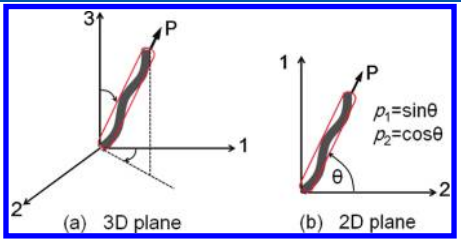

Figure 2. Definition of the direction of single MWNT by a unit vector **P** in the (a) 3D plane and (b) 2D plane, respectively. θ is the orientation angle of single MWNT in the 2D plane.

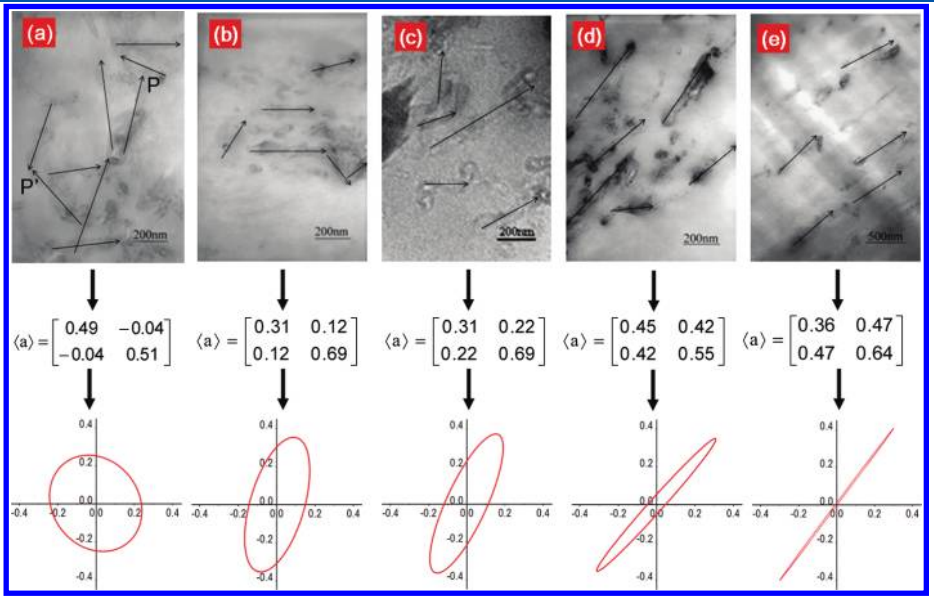

Figure 3. TEM images, second order orientation tensor, and ellipses of samples parallel to the tensile-strain direction in the MWNT/PVDF nanocomposites with 2.0 wt % MWNT, respectively: (a) TS = 0; (b) TS = 6.3%; (c) TS = 12.5%; (d) TS = 25.0%; (e) TS = 37.5%.

Table 1. Principal Values of the Second Order Orientation Tensor $\langle a \rangle^*$ and PAD Values at Different TSs

TS (%)	major axes length (a^*_{11})	minor axes length (a^*_{22})	φ in $\langle Q \rangle$	PAD
0	0.53	0.45	−52.0	0.08
6.3	0.72	0.28	73.9	0.44
12.5	0.79	0.21	65.4	0.58
25.0	0.92	0.07	48.4	0.85
37.5	0.99	0.01	53.3	0.98

tensile strain can strongly affect the MWNT redistribution once it goes into the plastic region, even exceeding the proportional limit slightly (ΔTS = 0.3%). (2) A much high PAD (>0.80) can be achieved only when the necking begins in the composite (at TS = 18.0%, Figure 1 and Table 1). From that point on, apart from the in-plane elongation, a significant out-of-plane geometric reduction also starts to contribute to the tube alignment until the composite is fractured.

Influence of Tensile Strain on the Dielectric Properties of MWNT/PVDF Nanocomposites. In order to examine the strain's impact on the dielectric properties, we choose composites with f_{MWNT} = 2.0 wt % to study, because this is in the vicinity of the threshold (f_c = 1.8 wt %) at which the dielectric behaviors would be much more sensitive to the microstructure shift and affected greatly by the external tensile strains. Figure 4 shows the dependence of dielectric properties on the frequency and tensile strain at room temperature. We first focus on the composite before stretching (TS = 0). As compared to the pure PVDF (Figure 4a), the percolation-type enhancement (10→300) in dielectric permittivity is visible (Figure 4b) and results from an insulation−conduction transition based on the network formation of MWNT clusters near f_c.[11,13,24,25] Additionally, the effect of interfacial polarization can be invoked as being responsible for the remarkable permittivity relaxation at low frequencies (10^2−10^4).[11,17] Nevertheless, after stretching, the dielectric properties exhibit a complicated changing law with TS ranging from 0 to 37.5%. As indicated in Figure 4b, the dielectric permittivity at low frequencies (10^2−10^4) would be affected more by strain than those at higher frequencies. In detail, although all the dielectric permittivity decreases with increasing frequency in the whole TS range, the significant low-frequency permittivity relaxation only appears at certain strain levels (TS = 0, 12.5%, 37.5%). A similar influence of the strain on the ac conductivity can be observed in Figure 4c; namely, low-frequency conductivity would be more sensitive to the TS variations than others at higher frequencies, showing a large variation of the flat plateau level of the curves (corresponding to the dc conductivity). However, the relaxation of ac conductivity is almost the same at different TSs. To give a detailed description of the changing law, dependences of the dielectric permittivity and ac conductivity on TS at 10^2 Hz are plotted in Figure 5a. It is noticeable that, with TS increasing from 0 to 37.5%, the dielectric permittivity initially begins to decrease dramatically at TS = 6.3%, following a remarkable increase to maximum value at TS = 12.5%, a significant decrease again at TS = 18.8%, and finally a gradual increase while TS is up to 37.5%. A nearly opposite rule happens to the variation of ac conductivity for the composites. The results indicate that, by employing the stretching method, in comparison with TS = 0, the increment in the dielectric permittivity of the f_{MWNT} = 2 wt % composite can reach 30%

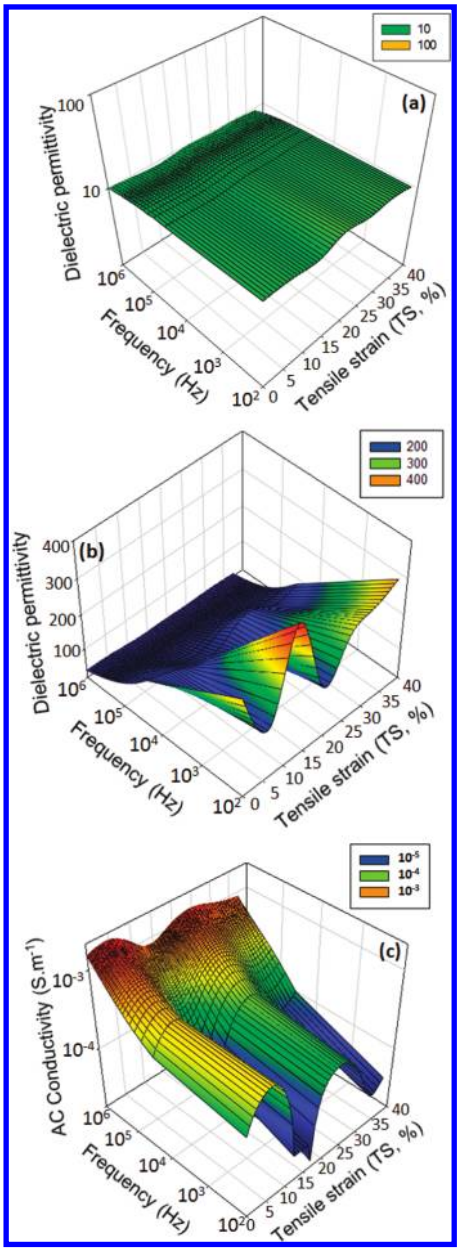

Figure 4. (a) Plots of the dielectric permittivity of pure PVDF against the frequency and tensile strain. Dependence of (b) the dielectric permittivity and (c) ac conductivity of the MWNT/PVDF nanocomposites with f_{MWNT} = 2 wt % on the frequency and tensile strain at room temperature.

at 10^2 Hz, and the corresponding ac conductivity decreases by 92%.

Correlation of the MWNT Alignment with the Dielectric Property Evolution. The following possible mechanisms can be suggested to explain the observed evolution of dielectric properties. A first possibility is associated with the PVDF matrix, i.e., the phase transition from α- to β-PVDF owing to the mechanical stretching.[31] Compared to the most common α-phase, the β-phase characterized by all-trans planar zigzag conformation with all the fluorine atoms located on the same side of the polymer chains can give PVDF a much higher polarity due to the net dipole moment.[31,32] Thus, a remarkable α- to β-phase transition would certainly change the dielectric properties of the composite.

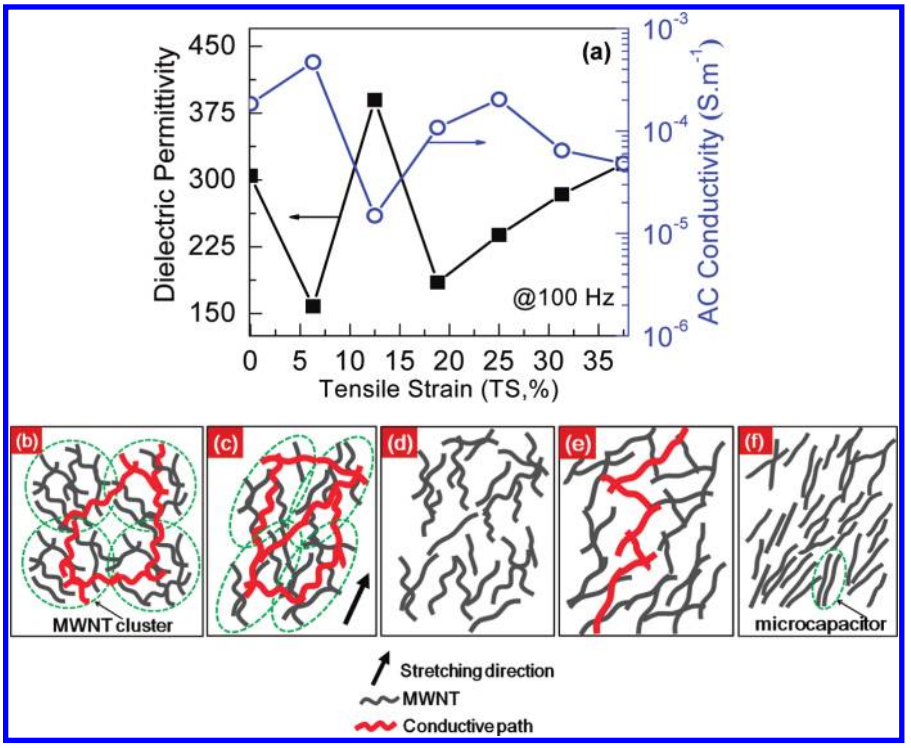

Figure 5. (a) Plots of the dielectric permittivity and ac conductivity at 10^2 Hz against the tensile strain, TS, for the f_{MWNT} = 2 wt % composites. (b−f) Schematic change of the MWNT distribution in the composite with (b) TS = 0, (c) TS = 6.3%, (d) TS = 12.5%, (e) TS = 18.8%, and (f) 18.8% < TS ≤ 37.5%, respectively.

However, according to the literature,[31,33−35] such phase transformation was basically achieved when PVDFs were stretched at a high temperature (70−100 °C) with a colossal tensile strain (200−400%). In our case, the tensile strain values are far below this transition-required level, even for the largest TS (37.5%). Therefore, the phase structure of the PVDF matrix remains stable during stretching, which can be further confirmed by the dependence of dielectric permittivity of pure PVDF on the frequency and strain (Figure 4a; at each frequency the dielectric permittivity remains nearly stable, regardless of the increase of TS). Hence, the strain effect on the dielectric properties of PVDF matrix can be neglected.

Recall that MWNT clusters and interfacial polarization play an important role in determining the dielectric properties of composites. Thereby, other mechanisms based on these two factors should be put forward. The evolution of conductive path and the formation of microcapacitor network made from the aligned MWNTs in the direction of tensile strain would take charge for the complex changes of dielectric properties in Figure 5a. When the composites are subject to a uniaxially stretching at a low strain level (TS = 6.3%), the original MWNT clusters can remain but be elongated, which has been evidenced by the sharp variation of the PAD of MWNTs (Table 1). This induces additional conductive paths between clusters (as illustrated in Figure 5c) and subsequently increases the conductivity (Figures 4c and 5a, TS = 6.3%). [There already exist conductive paths between original MWNT clusters (dashed circle area in Figure 5b) before stretching, because of the MWNT content higher than f_c,[24,25] as illustrated in Figure 5b.] The enhanced conductivity is nevertheless not desirable for preserving charges blocked at the MWNT-PVDF interfaces. Hence the permittivity relaxation becomes less significant and leads to a sharp decrease in permittivity (Figures 4b and 5a, TS = 6.3%). With TS increasing further, the elongated MWNT cluster would be largely destroyed and numerous fresh MWNT−PVDF interfaces form (MWNT−MWNT contacts change partially into MWNT-PVDF contacts) because of the continuous displacement of MWNT along the stretching direction (Figure 5d, TS = 12.5%). The damage of conductive paths between neighboring clusters would result in a dramatic decrease in conductivity. However, the enhanced interfacial polarization is prone to induce a much more remarkable relaxation at low frequency, leading to an increase in the dielectric permittivity (Figures 4b and 5a, TS = 12.5%). From a TS of 18.0% on, a high degree of MWNT alignment could be expected because of the occurrence of necking in the composites (Figure 1). The straightening of tube flexure enables heads of one MWNT meet ends of others, thus reconstructing conductive paths among individual MWNTs (Figure 5e). This would increase conductivity and decrease permittivity again (Figure 5a, TS = 18.8%). The high PAD level (>0.8) in this range (18.8−37.5%) signifies that MWNTs are highly oriented along the stretching direction, giving rise to a network of microcapacitor with the MWNTs as electrodes and a very thin PVDF layer in between (Figure 5f). For each microcapacitor, the capacitance, C, can be calculated by

$$C = \frac{\varepsilon_0 \varepsilon_r S}{d} \tag{6}$$

where ε_0 is the dielectric permittivity of the free space ($\varepsilon_0 \approx 8.854 \times 10^{-12}$ F m^{-1}), ε_r is the dielectric permittivity of PVDF, S is the area of overlap of the two MWNT electrodes, and d is the separation between the two electrodes. With TS increasing from 18.8% to 37.5%, the thickness of PVDF layers, d, would decrease gradually and improve the effective capacitance of both the microcapacitors and the whole composite, and then the

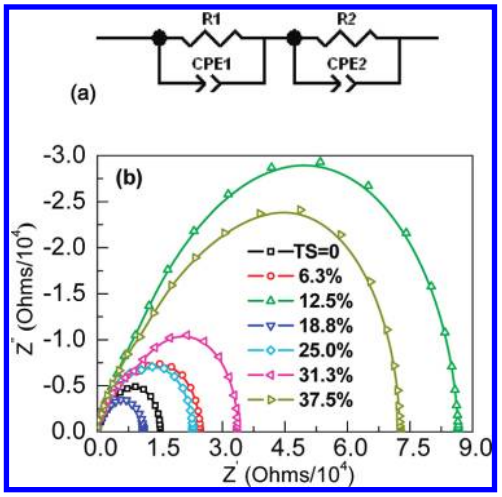

Figure 6. (a) Equivalent circuit of the MWNT/PVDF nanocomposites with f_{MWNT} = 2 wt % and (b) Nyquist plots of the composites at different TS.

composites' dielectric permittivity due to the proportional relationship between the permittivity and the capacitance as shown in eq 6.[36] However, the conductivity in this range (18.8−37.5%) does not vary with TS monotonously, possibly because of the local fluctuations in the distance between the neighboring MWNTs during stretching.

Impedance Analysis for the Composites at Different Tensile Stains. Dielectric properties of the CNT composite can also be explored by its equivalent circuit model composed of three elements: resistor (R), capacitor (C), and inductor (L) elements.[36,37] The polarization and ac conduction mechanisms can be revealed according to the basic composition elements of the composites.[37,38] To verify the above mechanisms for the dielectric evolution, we establish an equivalent circuit model of two parallel RC circuits in series for our MWNT/PVDF nanocomposites, as illustrated in Figure 6a. The constant phase elements (CPEs) are used to simulate the impedance data instead of the ideal capacitor. Figure 6b presents the Nyquist plots of the composites at different TS with frequency increasing from right (10^{-3} Hz) to left (10^{7} Hz). They are shown as half circles indicating the existence of interparticle current flow and the polarization resistance at interfaces.[37] The diameters of these semicircles correspond to the bulk resistivity of the composites at different TS levels. With the increase in TS, the variation of this resistivity is nearly identical to that in Figure 5a. For example, the Cole−Cole plot at TS of 12.5% has the largest diameter, meaning that the composite at this strain level possesses lowest conductivity, similar to Figure 5a. By using the Zview2 software, the impedance data of the sample can be analyzed and the parameters of equivalent circuits are calculated according to the following equation

$$Z^* = \frac{R}{1 + j\omega CR} = \frac{R}{1 + j\omega\tau} \quad (7)$$

where $\tau = RC$ is the time constant of circuits. The simulated values of each element by fitting the impedance data to the equivalent circuit are shown in Table 2. It should be emphasized that no semicircle has been experimentally observed for the Nyquist plot of the PVDF matrix, suggesting that the electrical polarization in composites is very concerned with MWNT additives.[39] Considering the great effect of interfacial polarization on the dielectric properties, it is reasonable to conclude that the adscription of CPE1 and CPE2 is to the MWNT polarization and MWNT−PVDF interface polarizations, respectively, as the value of CPE2 is an order of magnitude larger than that of CPE1. It should be also noted that the highest R values are obtained at TS = 12.5%, which is nearly consistent with the variation of conductivity in Figure 5a. Moreover, when the high PAD value is reached (e.g., TS = 37.5%), we obtain the high CPE2 values (Table 2), indicating the great contribution of the interfacial polarization to the macroscopic dielectric properties. Overall, the analysis of impedance spectra and the established equivalent circuit verifies the mechanisms proposed for the evolution of dielectric properties.

Table 2. Simulated Values of Each Element According to the Impedance Data and Equivalent Circuit in Figure 6a

TS (%)	R1 ($\Omega/10^5$)	CPE1 ($F/10^{-10}$)	R2 ($\Omega/10^5$)	CPE2 ($F/10^{-10}$)
0	0.53	4.83	0.51	21.63
6.3	0.29	2.67	0.25	11.81
12.5	16.85	3.66	3.23	19.27
18.8	1.93	1.92	0.37	21.95
25	0.70	3.51	0.59	23.68
31.3	2.46	5.06	1.86	14.73
37.5	3.50	3.11	0.99	35.47

CONCLUSIONS

In summary, a high-dielectric-permittivity MWNT/PVDF nanocomposite has been obtained. The orientation of the MWNTs inside the composites can be changed by uniaxial mechanical stretching. The nanotube orientation state was quantitatively characterized by using TEM as well as the second order orientation tensor at a selected location. A high alignment degree happened when the necking began in composites. The change of nanotube distribution state highly affected the dielectric properties. A correlation of the tube orientation state with the evolution of dielectric properties was established. With increasing the alignment degree of nanotubes, the dielectric permittivity and ac conductivity exhibited complex but nearly opposite changing tendency. This could be attributed to the conductive pathways shift and microcapactor formation during the tensile deformation. This was further confirmed by using an equivalent circuit model of two parallel RC circuits in series to analyze the impedance data. Overall, we hope that our study would form a helpful reference to predict the strain-induced changes of dielectric properties of electroactive composites in practical applications.

AUTHOR INFORMATION

Corresponding Author
*Phone: +86-10-62332599 (Z.-M.D.); +33-141131316 (J.B.). E-mail address:dangzm@ustb.edu.cn (Z.-M.D.);address:jinbo.bai@ecp.fr (J.B.).

ACKNOWLEDGMENT

This work was financially supported by the NSF of China (Grant 50977001), the State Key Laboratory of Power System

(SKLD09KZ03), the Ministry of Sciences and Technology of China through 863-project (Grant 2008AA03Z307), the Program for New Century Excellent Talents in University (NCET), the Ministry of Sciences and Technology of China through China−Europe International Incorporation Project (Grant 2010DFA51490), and the Project-sponsored by SRF for ROCS, SEM. S.-H.Y. and J.-K.Y. thank the Eiffel fellowship and CSC scholarship, respectively.

REFERENCES

(1) Ajayan, P. M.; Stephan, O.; Colliex, C.; Trauth, D. *Science* **1994**, *265*, 1212.
(2) Tans, S. J.; Verschueren, A. R. M.; Dekker, C. *Nature* **1998**, *393*, 49.
(3) Berber, S.; Kwon, Y. K.; Tomanek, D. *Phys. Rev. Lett.* **2000**, *84*, 4613.
(4) Pop, E.; Mann, D.; Wang, Q.; Goodson, K.; Dai, H. *Nano Lett.* **2006**, *6*, 96.
(5) Coleman, J. N.; Khan, U.; Gun'ko, Y. K. *Adv. Mater.* **2006**, *18*, 689.
(6) Sreekumar, T. V.; Liu, T.; Min, B. G.; Guo, H.; Kumar, S.; Hauge, R. H.; Smalley, R. E. *Adv. Mater.* **2004**, *16*, 58.
(7) Huang, H.; Liu, C. H.; Wu, Y.; Fan, S. S. *Adv. Mater.* **2005**, *17*, 1652.
(8) Yang, Y.; Gupta, M. C.; Dudley, K. L.; Lawrence, R. W. *Nano Lett.* **2005**, *11*, 2131.
(9) Huang, Y. Y.; Terentjev, E. M. *Adv. Funct. Mater.* **2010**, *20*, 4062.
(10) Wu, J.; Kong, L. *Appl. Phys. Lett.* **2004**, *84*, 4956.
(11) Wang, L.; Dang, Z. *Appl. Phys. Lett.* **2005**, *87*, 042903.
(12) Yuan, J. K.; Li, W. L.; Yao, S. H.; Lin, Y. Q.; Sylvestre, A.; Bai, J. *Appl. Phys. Lett.* **2011**, *98*, 032901.
(13) Zhang, S. H.; Zhang, N. Y.; Cheng, H.; Ren, K. L.; Zhang, Q. M. *Adv. Mater.* **2005**, *17*, 1897.
(14) Dang, Z. M.; Wang, L.; Yin, Y.; Zhang, Q.; Lei, Q. Q. *Adv. Mater.* **2007**, *19*, 852.
(15) Zhang, Q. M.; Li, H.; F.; Poh, M.; Xia, F.; Cheng, Z. Y.; Xu, H. S.; Huang, C. *Nature* **2002**, *419*, 284.
(16) Huang, C.; Klein, R.; Xia, F.; Li, H.; Zhang, Q. M.; Bauer, F.; Cheng, Z. Y. *IEEE Trans. Dielectr. Electr. Insul.* **2004**, *11*, 299.
(17) Yuan, J. K.; Yao, S. H.; Dang, Z. M.; Sylvestre, A.; Genestoux, M.; Bai., J. *J. Phys. Chem. C* **2011**, *115*, 5515.
(18) Baughman, R. H.; Zakhidov, A. A.; De Heer, W. A. *Science* **2002**, *297*, 787.
(19) Jin, L.; Bower, C.; Zhou, O. *Appl. Phys. Lett.* **1998**, *73*, 1197.
(20) Choi, E. S.; Brooks, J. S.; Eaton, D. L.; Al-Haik, M. S.; Hussaini, M. Y.; Garmestani, H.;; et al. *J. Appl. Phys.* **2003**, *94*, 6034.
(21) Abdalla, M.; Dean, D.; Theodore, M.; Fielding, J.; Nyairo, E.; Price, G. *Polymer* **2010**, *51*, 1614.
(22) Park, C.; Wilkinson, J.; Banda, S.; Ounaies, Z.; Wise, K. E.; Sauti, G.;; et al. *J. Polym. Sci., Part B: Polym. Phys.* **2006**, *44*, 1751.
(23) Zhang, C.; Zhu, J.; Ouyang, M.; Ma, C. *Appl. Phys. Lett.* **2009**, *94*, 111915.
(24) Yao, S. H.; Dang, Z. M.; Xu, H. P.; Jiang, M. J.; Bai, J. *Appl. Phys. Lett.* **2008**, *92*, 082902.
(25) Yao, S. H.; Dang, Z. M.; Jiang, M. J.; Xu, H. P.; Bai, J. *Appl. Phys. Lett.* **2007**, *91*, 212901.
(26) Advani, S. G; Tucker, C. L. *J. Rheol.* **1990**, *34*, 367.
(27) Tucker, C. L.; Advani, S. G. *Processing of Short-Fiber Systems. Flow and Rheology in Polymer Composites Manufacturing*; Elsevier: Amsterdam, 1994.
(28) Fan, Z. H.; Advani., S. G. *Polymer* **2005**, *46*, 5232.
(29) Bhattacharyya, A. R.; Sreekumar, T. V.; Liu, T.; Kumar, S.; Ericson, L. M.; Hauge, R. H.;; et al. *Polymer* **2003**, *44*, 2373.
(30) Hobbie, E. K; Wang, H.; Kim, H.; Han, C. C.; Grulke, E. A.; Obrzut, J. *Rev. Sci. Instrum.* **2003**, *74*, 1244.
(31) Sun, L. L.; Li, B.; Zhang, Z. G.; Zhong, W. H. *Eur. Polym. J.* **2010**, *46*, 2112.
(32) Yuan, J. K.; Dang, Z. M.; Yao, S. H.; Zha, J. W.; Zhou, T.; Li, S. T.; Bai., J. *J. Mater. Chem.* **2010**, *20*, 2441.
(33) Broahurst, M. G.; Davis, G. T.; McKinney, J. E.; Collins, R. E. *J. Appl. Phys.* **1978**, *49*, 4992.
(34) ElMohajir, B. E.; Heymans, N. *Polymer* **2001**, *42*, 5661.
(35) Sajkiewicz, P.; Wasiak, A.; Golclowski, Z. *Eur. Polym. J.* **1999**, *35*, 423.
(36) Jiang, M. J.; Dang, Z. M.; Bozlar, M.; Miomandre, F.; Bai, J. *J. Appl. Phys.* **2009**, *106*, 084902.
(37) Dang, Z. M.; Yao, S. H.; Yuan, J. K.; Bai, J. *J. Phys. Chem. C* **2010**, *114*, 13204.
(38) Jonscher, A. K. *Universal Relaxation Law*; London: Chelsea Dielectric, 1992.
(39) Yao, S. H.; Yuan, J. K.; Dang, Z. M.; Bai, J. *Mater. Lett.* **2010**, *64*, 2682.